



A fundamental study on the pyrolysis of hydrocarbons

Shashank S. Nagaraja, Amrit B. Sahu*, Snehasish Panigrahy, Henry J. Curran

Combustion Chemistry Centre, School of Chemistry, Ryan Institute, MaREI, National University of Ireland Galway, Ireland

ARTICLE INFO

Article history:

Received 20 February 2021

Revised 19 June 2021

Accepted 22 June 2021

Keywords:

Pyrolysis
Natural gas
Hydrocarbon
Alkane
Olefin
Alkene

ABSTRACT

A newly developed detailed chemical kinetic mechanism, NUIGMech1.1, is used to study the pyrolysis of $C_1 - C_7$ hydrocarbons at a constant initial fuel concentration in the temperature range 900 – 2000 K. We observe that, for a given reaction time and pressure, fuel pyrolysis does not occur below a certain “threshold temperature”. This phenomenon is explored further in this study by performing rate of production analyses for different fuels. It is observed that pyrolysis is highly sensitive to unimolecular dissociation reactions and that the products of unimolecular dissociation determine the secondary fuel consumption pathways. Furthermore, a minimum progress of reaction factor for the initiation of pyrolysis is established for different fuels over a wide range of residence time (3 ms – 30 min) and partial pressure (0.02 – 2.00 bar) conditions. This limiting factor determines the threshold temperature for the pyrolysis of any alkane or alkene. A computer program is developed based on this concept to calculate the threshold temperature. An application of threshold temperature is also illustrated.

© 2021 The Authors. Published by Elsevier Inc. on behalf of The Combustion Institute. This is an open access article under the CC BY license (<http://creativecommons.org/licenses/by/4.0/>)

1. Introduction

Pyrolysis is the chemical decomposition of organic materials through the application of heat. In recent times, pyrolysis processes have become popular due to their importance in the conversion of biomass and waste to other useful chemical products. Pyrolysis breaks down organic materials in the absence of oxygen to produce liquid (bio-oil), gaseous (hydrogen/syngas), and solid (biochar) products [1]. Pyrolysis is applied in a wide array of fields including waste management, material synthesis, soil amendment and energy generation. The design of a pyrolysis reactor and its operating conditions depends on the desired type of output product whose yield efficiency is controlled by residence time, heat supply rate and heat transfer [2,3]. Bridgewater [4] broadly classified pyrolysis into three categories depending on the operating temperature (T) and residence time (τ_{res}): slow pyrolysis ($\tau_{res} > 10$ min, low $T \sim 290 - 400$ K), intermediate pyrolysis ($\tau_{res} \sim 10 - 30$ s, moderate $T \sim 500$ K), fast pyrolysis ($\tau_{res} \sim 1$ s, moderate $T \sim 500$ K).

Energy generation from different hydrocarbon fuels occurs through combustion and gasification. Pyrolysis studies of different fuels are important in understanding combustion and gasification because, at higher temperatures, fuels first undergo pyrolytic reactions as an initiation step, and these are followed by the oxidation of the smaller species produced. The timescales of these

initial pyrolysis reactions during a combustion process are significantly faster (in the order of ms) compared to the processes discussed above. Typically, during pyrolysis, unimolecular dissociation reactions initiate the reactions followed by H-atom abstraction and addition reactions by hydrogen (\dot{H}) atoms and methyl ($\dot{C}H_3$) radicals.

Pyrolysis reactions have been studied by various groups. Nagaraja et al. studied the pyrolysis of $C_2 - C_6$ 1-alkenes, pentene isomers and allylic hydrocarbons in a single pulse shock tube at 2 ± 0.16 bar [5–7]. Methane pyrolysis was recently studied by Nativel et al. [8] at 1.5 bar. Additionally, Hidaka et al. studied ethane and propane pyrolysis [9,10]. Furthermore, Yasunaga et al. studied the pyrolysis of pentane, hexane and heptane [11] at an average pressure of ~ 2 bar. Bradley et al. [12] studied the pyrolysis of neopentane at pressures of 3 – 4 bar and Malewicki et al. studied the pyrolysis of higher alkanes including isooctane, decane and dodecane at relatively high pressures of 50 – 60 bar [13,14]. Plotting all of these experimental results together in Fig. 1, it can be seen that methane is the slowest fuel to decompose followed by ethylene and then propene and isobutene. Thereafter, other larger hydrocarbons are faster to pyrolyze until a “threshold temperature” (~ 950 K) is reached below which all of these hydrocarbons do not decompose at these conditions of fuel partial pressure and residence time. Details of the operating conditions for the fuels are provided in Table 1.

To our knowledge, the apparent existence of a threshold pyrolysis temperature has not been reported in the literature. Moreover, the following questions arise from Fig. 1:

* Corresponding author.

E-mail address: amritbikram.sahu@nuigalway.ie (A.B. Sahu).

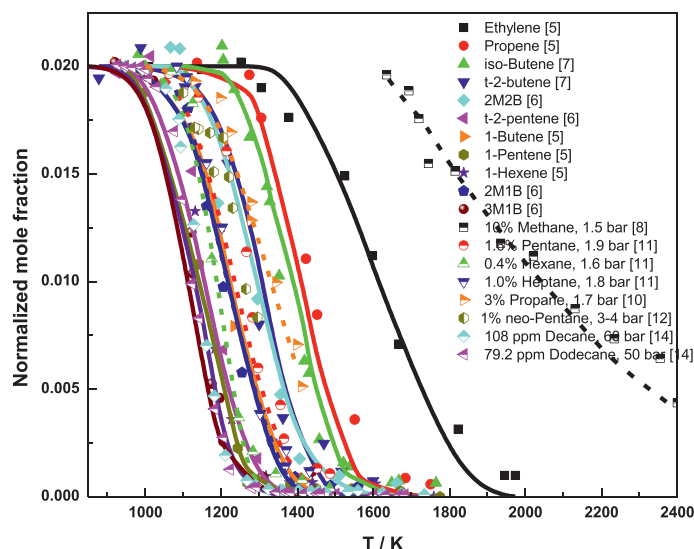


Fig. 1. Fuel normalized mole fraction profiles obtained from pyrolysis studies in the literature. Symbols: Experimental data. Lines: NUIGMech1.1 predictions. Residence times for these fuels are different and are provided in Table 1.

Table 1

Mole fraction, pressure and residence times of different fuels studied.

Fuel	Mole fraction (%)	Pressure (bar)	Residence time (ms)
Ethylene	2.0	2.0	3 – 4
Propene	2.0	2.0	3 – 4
isoButene	2.0	2.0	3 – 4
t-2-Butene	2.0	2.0	3 – 4
2M2B	2.0	2.0	3 – 4
t-2-Pentene	2.0	2.0	3 – 4
1-Butene	2.0	2.0	3 – 4
1-Pentene	2.0	2.0	3 – 4
1-Hexene	2.0	2.0	3 – 4
2M1B	2.0	2.0	3 – 4
3M1B	2.0	2.0	3 – 4
Methane	10.0	1.5	2.4 – 4
Pentane	1.6	1.9	1.5 – 1.8
Hexane	0.4	1.6	1.7 – 2.2
Heptane	1.0	1.8	1.7 – 2
Propane	3.0	1.7	1.9 – 2.5
neoPentane	1.0	3 – 4	0.6 – 1.1
Decane	0.0108	60	1.2 – 1.8
Dodecane	0.00792	50	1.2 – 2.4

- Why is methane so much slower to decompose compared to all of the other fuels?
- Why is ethylene slower to decompose compared to propene, isobutene, etc.?
- Propene and isobutene show very similar reactivities, with propene being slightly slower. Why? Is it primarily due to unimolecular dissociation or do subsequent allylic radical decompositions contribute to fuel reactivity?
- There is a limiting temperature below which the fuels do not decompose. It is observed that in flow and jet-stirred reactors, fuel reactivity is generally not sensitive to unimolecular fuel decomposition reactions at the temperatures (600–1000 K) and timescales (~ms–s) involved. In shock tubes ($T > 1000$ K at times in the μ s–ms timescale) ignition delay time predictions are very sensitive to unimolecular decomposition reactions [15]. Why is this?
- Is there a “limiting threshold temperature” for all hydrocarbon fuels? If so, why is this, and what is this temperature at a given pressure and reaction time?

In the current study, we attempt to evaluate and understand the behavior of all these fuels using a detailed chemical kinetic model. Based on our analyses, we also propose a parameter to predict the feasibility of fuel pyrolysis for any given operating condition.

2. Chemical kinetic simulations

Simulations are performed using CHEMKIN-Pro [16] assuming a closed homogeneous batch reactor at constant volume. A newly formulated $C_0 - C_7$ mechanism, NUIGMech1.1 [5,6,17–19], that has been validated against a wide range of experimental data [5,6,17,18] is used for our analysis in this study. The mechanism is also available at Prof. Henry Curran’s group webpage (<http://c3.nuigalway.ie/combustionchemistrycentre/mechanismdownloads/>).

3. Analysis of different hydrocarbons

We endeavor to correlate the temperature at which pyrolysis begins for $C_1 - C_7$ hydrocarbons and determine the rate of the initiation reaction(s) which include the unimolecular dissociation reaction(s) and other important secondary reactions of the fuel. The simulations are performed at 2 bar for 2% fuel diluted in argon at different reaction times in the temperature range 900 – 2000 K.

The fuel mole fraction profiles are shown in Fig. 2(a) and the unimolecular dissociation rate constants at 2 bar are provided in Fig. 2(b). Methane has the lowest reactivity, followed by ethylene and then propene and isobutene with 3-methyl-1-butene (3M1B) having the highest reactivity among the hydrocarbons studied. For a given temperature, the reaction of $CH_4 (+M) \rightarrow \dot{C}H_3 + H (+M)$ has the lowest rate constant followed by the unimolecular dissociation rate constants of ethylene, propene and isobutene. 3M1B and 1-pentene have the highest unimolecular dissociation rate constants at a given temperature. Moreover, propene and isobutene have similar unimolecular dissociation rate constants and hence their pyrolytic initiation is similar at 2 bar. Thus, fuel decomposition is initially controlled by the unimolecular dissociation rate and later by secondary reactions. Furthermore, it appears that there is a limiting rate below which pyrolysis does not/will not occur for a given reaction time. We explored this further by defining a threshold temperature and using equal rate constants for the unimolecular dissociation of alkanes.

3.1. Threshold temperature for fuel pyrolysis

We refer to the temperature at which fuel pyrolysis begins as the “threshold temperature” (T_{thres}) and have determined it by performing simulations for each fuel in the range 900 – 2000 K at a fixed initial fuel concentration, pressure and reaction time. The temperature at which the tangent to the fuel mole fraction (χ) gradient with respect to temperature ($d\chi/dT$) intercepts the T -axis is defined as the “threshold temperature”. Figure 3 illustrates T_{thres} for propene (1180 K) and 1-butene (1020 K) pyrolysis at 2% initial fuel concentration, 2 bar pressure and a reaction time of 3.25 ms. The values for methane (CH_4), propane (C_3H_8), n -butane ($n-C_4H_{10}$), isobutane ($i-C_4H_{10}$), neopentane ($neoC_5H_{12}$), n -pentane ($n-C_5H_{12}$), isopentane ($i-C_5H_{12}$), n -heptane ($n-C_7H_{16}$), 3-methyl-1-butene (cC_5H_{10}), 1-butene ($1-C_4H_8$), 2-methyl-1-butene (aC_5H_{10}), 1-pentene ($1-C_5H_{10}$), propene (C_3H_6), isobutene ($i-C_4H_8$) and 2-methyl-2-butene (bC_5H_{10}) are all provided in Table 2, together with their associated unimolecular dissociation type which can be C–C, alkane C–H or allylic C–H bond cleavage.

3.2. Impact of unimolecular dissociation reaction

In order to demonstrate that the rate constant for unimolecular dissociation (UMD) controls fuel decomposition, we have forced

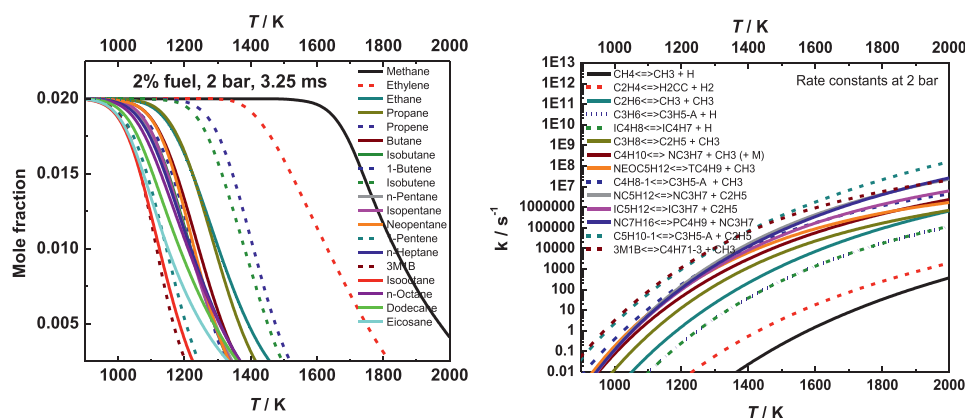


Fig. 2. (a) Fuel mole fraction profiles of $C_1 - C_7$ hydrocarbons at $p = 2$ bar and $\tau_{res} = 3.25$ ms. (b) Unimolecular dissociation rate constants for the different fuels studied at 2 bar.

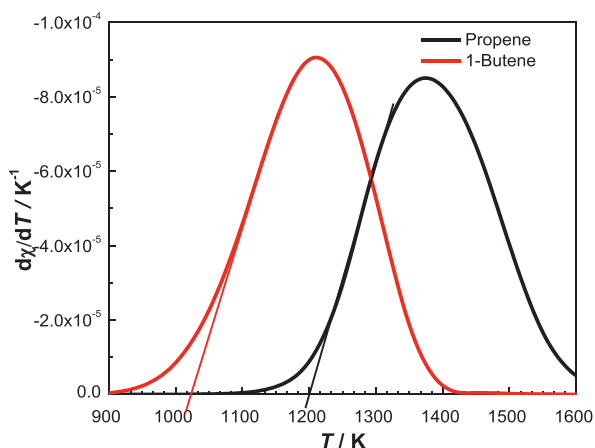


Fig. 3. Calculation of threshold temperature for propene and 1-butene at 2 bar, 3.25 ms reaction time and 2% initial fuel concentration.

Table 2

Threshold temperatures for different fuels at 2 bar, 2% fuel concentration and 3.25 ms residence time. A species glossary is provided as Supplementary material.

Fuel	Initiation reaction (s)	Dissociation type	Threshold temperature (K)
CH_4	$CH_4 \leftrightarrow \dot{C}H_3 + \dot{H}$	alkane C-H	1570
C_3H_8	$C_3H_8 \leftrightarrow \dot{C}_2H_5 + \dot{C}H_3$	C-C	1075
$n-C_4H_{10}$	$C_4H_{10} \leftrightarrow n\dot{C}_3H_7 + \dot{C}H_3$	C-C	1030
	$C_4H_{10} \leftrightarrow \dot{C}_2H_5 + \dot{C}_2H_5$		
$i-C_4H_{10}$	$iC_4H_{10} \leftrightarrow i\dot{C}_3H_7 + \dot{C}H_3$	C-C	1005
$neoC_5H_{12}$	$neoC_5H_{12} \leftrightarrow t\dot{C}_4H_9 + \dot{C}H_3$	C-C	1030
$n-C_5H_{12}$	$nC_5H_{12} \leftrightarrow n\dot{C}_4H_9 + \dot{C}H_3$	C-C	1000
$i-C_5H_{12}$	$iC_5H_{12} \leftrightarrow i\dot{C}_4H_9 + \dot{C}H_3$	C-C	1000
$n-C_7H_{16}$	$nC_7H_{16} \leftrightarrow n\dot{C}_6H_{13} + \dot{C}H_3$	C-C	990
cC_5H_{10}	$3M1B \leftrightarrow \dot{C}_4H_7-1,3 + \dot{C}H_3$	C-C	960
$1-C_4H_8$	$1-C_4H_8 \leftrightarrow \dot{C}_3H_5-a + \dot{C}H_3$	C-C	1020
aC_5H_{10}	$2M1B \leftrightarrow i\dot{C}_4H_7 + \dot{C}H_3$	C-C	1000
$1-C_5H_{10}$	$1-C_5H_{10} \leftrightarrow \dot{C}_4H_9-a + \dot{C}_2H_5$	C-C	950
C_3H_6	$C_3H_6 \leftrightarrow \dot{C}_3H_5-a + \dot{H}$	allylic C-H	1180
$i-C_4H_8$	$i-C_4H_8 \leftrightarrow i\dot{C}_4H_7 + \dot{H}$	allylic C-H	1160
bC_5H_{10}	$2M2B \leftrightarrow a\dot{C}_5H_9-c + \dot{H}$	allylic C-H	1080
	$2M2B \leftrightarrow c\dot{C}_5H_9-b + \dot{H}$		

the rate for the unimolecular dissociation of methane, ethane, n -butane, n -pentane and n -heptane to be the same as that for propane. Figure 4(a) compares the fuel mole fraction profiles for these fuels with that predicted for propane. The decomposition profiles for all of the higher alkanes move to higher temperatures and get slower with all of them lying within ~ 50 K of that ob-

served for C_3H_8 , while those for methane and ethane get faster and approach that predicted for propane. Further differences within different fuel profiles are attributed to differences in the rate constants for H-atom abstraction by \dot{H} atoms and $\dot{C}H_3$ radicals.

The most noticeable change in the trend in reactivity is observed for CH_4 which also shows the largest sensitivity to the unimolecular decomposition reaction. The threshold temperature for methane decreases by ~ 240 K from 1550 K to 1310 K but remains ~ 225 K larger than the threshold temperature determined for C_3H_8 pyrolysis. Assigning a rate constant for the UMD of CH_4 to be equal to that for C_3H_8 leads to the dashed black line depicted in Fig. 4(b) which is not very comparable to the C_3H_8 decomposition profile, therefore showing that secondary (abstraction) reactions are also very important. It is found that when the decomposition of methane, $CH_4 (+M) \leftrightarrow \dot{C}H_3 + \dot{H} (+M)$, is further forced in the forward direction only, its concentration profile (black dash-dotted line) almost overlaps with that of C_3H_8 (red solid line) as shown in Fig. 4(b). Thus, for methane, the reaction $CH_4 (+M) \leftrightarrow \dot{C}H_3 + \dot{H} (+M)$ is in equilibrium, maintaining a steady rate of production and consumption of \dot{H} atoms. However, no such change in the C_3H_8 profile is observed when the primary UMD reaction $C_3H_8 (+M) \leftrightarrow \dot{C}H_3 + \dot{C}_2H_5 (+M)$ is included in the forward direction only. This is because on production, \dot{C}_2H_5 radicals decompose to ethylene and \dot{H} atoms and thus no similar equilibrium can be established for propane, or any other higher alkane, as that observed for methane.

To support this, the species concentration profiles for CH_4 and the subsequent primary unimolecular dissociation products, i.e. $\dot{C}H_3$ and \dot{H} are plotted as a function of time in Fig. 5(a). Initially, CH_4 undergoes unimolecular dissociation producing $\dot{C}H_3$ and \dot{H} leading to an increase in their concentrations. \dot{H} atoms abstract H-atoms from the fuel producing $\dot{C}H_3$ and H_2 , therefore leading to an increase in $\dot{C}H_3$ radical concentrations with simultaneously declining \dot{H} atom concentrations. In this intermediate phase, at $\tau = 10^{-7} - 10^{-5}$ s, we also observe a reduction in the contribution to fuel consumption of the unimolecular decomposition reaction, Fig. 5(a). In contrast, our analysis for C_3H_8 , Fig. 5(b), shows that after the initial phase, UMD becomes less important ($< 10\%$) to fuel consumption. The change in trends of UMD reaction contribution are marked by the vertical dashed lines included in Figs. 5 and 6. Moreover, it should be noted that the primary products of C_3H_8 dissociation, $\dot{C}H_3$ and \dot{C}_2H_5 radicals, do not exhibit a simultaneous increase in their concentrations as observed for CH_4 consumption as \dot{C}_2H_5 radicals decompose to ethylene and \dot{H} atoms. Subsequently, \dot{H} atoms and $\dot{C}H_3$ radicals abstract H-atoms from the fuel, together controlling $> 90\%$ of C_3H_8 consumption. In the initial phase, at $\tau = 10^{-9} - 10^{-7}$ s for the two fuels, where unimolecular

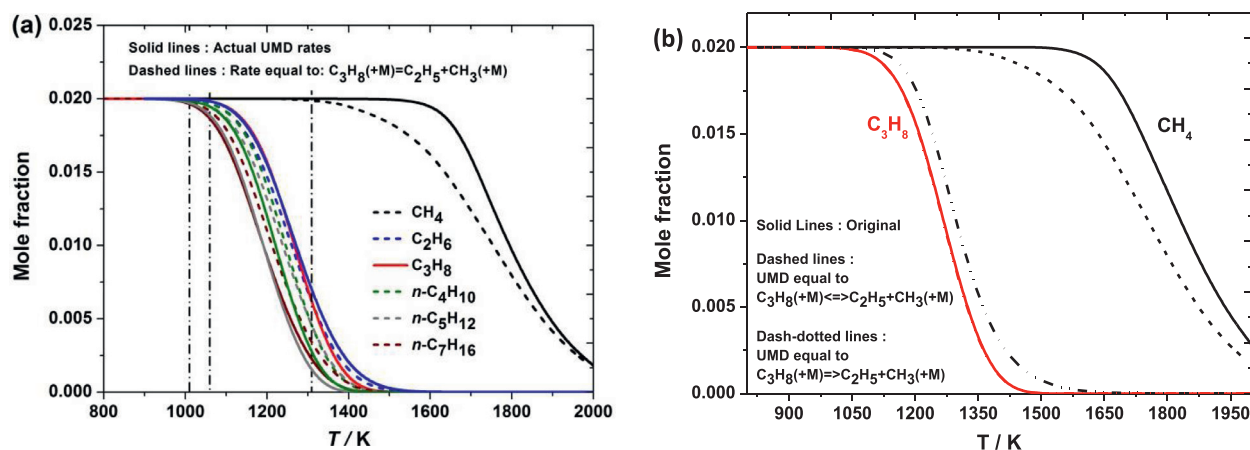


Fig. 4. (a) Fuel mole fraction profiles of C_1 to C_7 hydrocarbons with unimolecular dissociation reaction channel equal to $C_3H_8 (+M) \leftrightarrow \dot{C}_2H_5 + \dot{C}H_3 (+M)$, $p = 2$ bar, $\tau_{res} = 3.25$ ms. (b) Comparison of CH_4 and C_3H_8 fuel mole fraction profiles with reversible (\leftrightarrow) and irreversible (\Rightarrow) fuel decomposition reactions. (For interpretation of the references to color in this figure, the reader is referred to the web version of this article.)

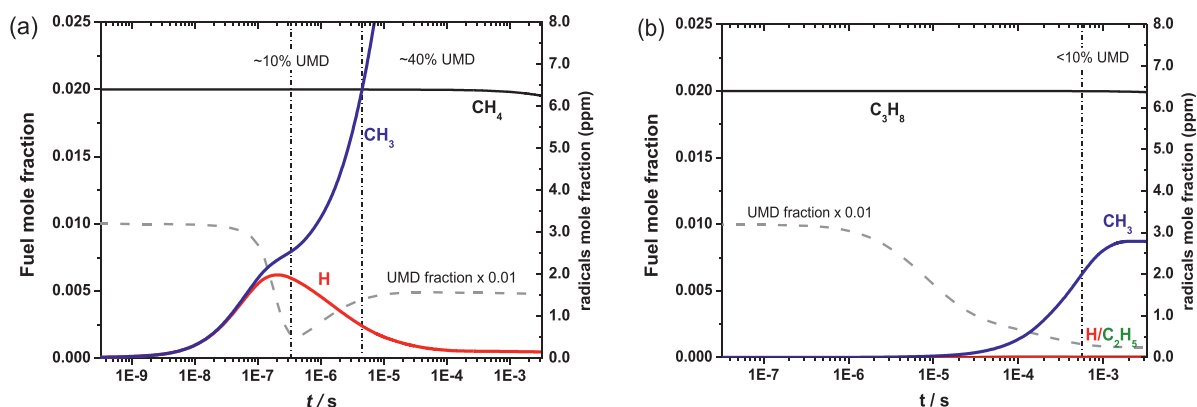


Fig. 5. Fuel and primary dissociation products species concentration profiles as a function of time for (a) CH_4 at $T = 1350$ K and (b) C_3H_8 at $T = 1050$ K, $p = 2$ bar. Solid lines represent species mole fraction and the dashed line shows the relative contribution of UMD towards fuel consumption. Vertical dashed lines indicate changes in contribution of UMD reactions.

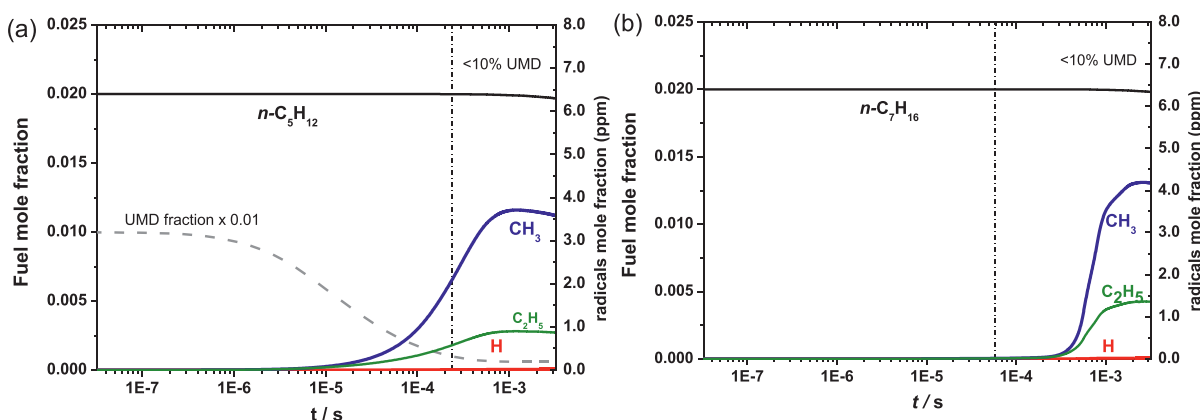


Fig. 6. Fuel and primary dissociation products species concentration profiles as a function of time for (a) $n-C_5H_{12}$ at $T = 1050$ K and (b) $n-C_7H_{16}$ at $T = 1050$ K, $p = 2$ bar. Solid lines represent species mole fraction and the dashed line shows the relative contribution of UMD towards fuel consumption. Vertical dashed lines mark the time beyond which contribution of UMD is less than 10%.

decomposition reaction is the dominant channel, we observe that in the case of CH_4 , both the primary dissociation radical products ($\dot{C}H_3$ and H) are in relatively high concentration.

The primary dissociation products for higher alkanes, Fig. 6(a) and (b) also follow the same trend as those for C_3H_8 , and therefore the reverse reactions do not have any impact on any of their fuel concentration profiles.

Furthermore, even though the reaction $CH_4 + \dot{C}H_3 \leftrightarrow \dot{C}H_3 + CH_4$ may occur the net effect is zero, and thus the reaction is not included in the mechanism. This is not true for any other fuel where $\dot{C}H_3$ will have a net positive effect on fuel consumption via the generic reaction $RH + \dot{C}H_3 \leftrightarrow \dot{R} + CH_4$. Additionally, methyl-methyl recombination acts as a chain termination reaction and is also observed to have an impact on T_{thres} , albeit

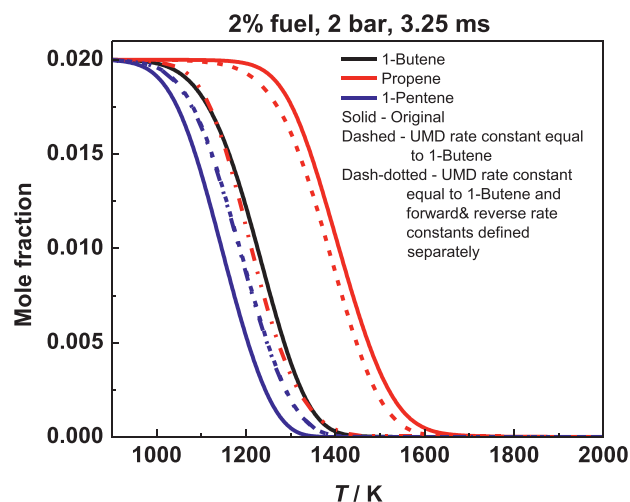


Fig. 7. Fuel mole fraction profiles of C_3 to C_5 1-alkenes with unimolecular dissociation reaction channel equal to $1-C_4H_8 (+M) \leftrightarrow \dot{C}_3H_5-a + \dot{C}H_3 (+M)$, $p = 2$ bar, $\tau_{res} = 3.25$ ms.

small, under these conditions. Therefore, methane decomposition is much slower than for all other alkanes primarily due to the net zero effect of H-atom abstraction by $\dot{C}H_3$ radicals, the relatively higher BDE for the alkane C-H bond compared to a C-C bond, and the quasi equilibrium established in the intermediate phase ($\tau = 10^{-7} - 10^{-5}$ s, Fig. 5(a)).

In the case of alkenes, the UMD rate constants of propene and 1-pentene were modified to be equal to that used for 1-butene, Fig. 7. The dashed lines represent simulations where the forward reaction parameters for propene and 1-pentene are taken to be equal to that for $1-C_4H_8 (+M) \leftrightarrow \dot{C}_3H_5-a + \dot{C}H_3 (+M)$, while the reverse rate constants were calculated based on the parent fuels' thermochemistry. The dash-dotted lines represent simulations where the forward and reverse reaction parameters were set equal to the rate constant for the reaction $1-C_4H_8 (+M) \leftrightarrow \dot{C}_3H_5-a + \dot{C}H_3 (+M)$. On implementing equal rate constants for these fuels, the fuel profiles shift closer to one another. Further differences within different fuel profiles are attributed to differences in the rate constants of the secondary H-atom abstraction and smaller radical decomposition reactions. In the case of propene, assigning a rate constant equal to that for 1-butene does not lead to a comparable decomposition profile. It was found that when the forward and reverse reactions of propene UMD are defined separately, the C_3H_6 mole fraction profile (red dash-dotted line) almost overlaps with that of 1-butene (black solid line) as shown in Fig. 7. However, no such change in the 1-pentene profile is observed when similar changes are made in its primary UMD reaction. Allyl radicals are produced by UMD and H-atom abstraction reactions in the case of propene which is not the case for other alkenes. Hence, due to the abundance of allyl radicals, a quasi-equilibrium is established slowing down the consumption of propene. This can be observed in Fig. 8. The UMD of propene produces allyl radicals and H atoms. A study was performed where the rate constant of the UMD reaction was allowed to be reversible and then irreversible. Initially, no difference is seen between the reversible (black lines) and irreversible (red lines) cases (Fig. 8). At times longer than 5×10^{-7} s, it is observed that the reaction $\dot{C}_3H_5-a + \dot{H} \leftrightarrow C_3H_6$ contributes to fuel consumption as indicated by the rise in the concentrations of \dot{C}_3H_5-a and H atoms.

Furthermore, in the above analyses, it was observed that along with the reactions, secondary reactions also contribute to the fuel consumption at T_{thres} . Therefore, an integrated flux analysis was performed to comprehend the importance of the secondary reactions.

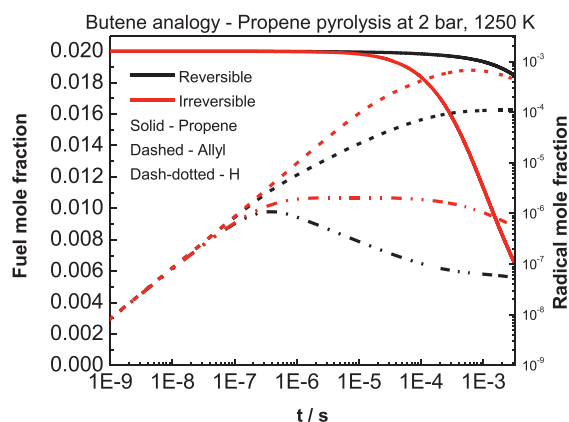


Fig. 8. Fuel and radical mole fractions for propene pyrolysis using the 1-butene UMD rate constant at $p = 2$ bar, $T = 1250$ K and $\tau = 3.25$ ms. (For interpretation of the references to color in this figure, the reader is referred to the web version of this article.)

3.3. Integrated flux analysis/sensitivity analysis

3.3.1. Analysis of alkane pyrolysis

To determine the fuel consumption pathways at the threshold temperatures, integrated reaction flux analyses were conducted for the consumption of each fuel. Figure 9(a) shows comparisons of the contributions of various channels for methane, ethane, propane, *n*-butane, *n*-pentane, and *n*-heptane at 2 bar at their corresponding threshold temperatures. In the case of methane approximately 40% of the total fuel consumption occurs through unimolecular decomposition while the remaining is via H-atom abstraction by H atoms. For propane and higher alkanes, the unimolecular decomposition channel only contributes approximately 8 – 15%, while the major flux occurs via H-atom abstraction by H atoms (41– 61%) and $\dot{C}H_3$ radicals (31 – 43%). Ethane exhibits an anomalous behavior where H-atom abstraction by H atoms is responsible for almost 97% of the total fuel consumption, while the unimolecular decomposition channel is limited to only ~1%. For ethane, unimolecular dissociation only produces methyl radicals, $C_2H_6 (+M) \rightarrow \dot{C}H_3 + \dot{C}H_3 (+M)$. These radicals abstract hydrogen from ethane creating ethyl (\dot{C}_2H_5) radicals. As soon as ethyl radicals are formed, a self-sustaining loop of $C_2H_6 + \dot{H} \rightarrow \dot{C}_2H_5 + H_2$ and $\dot{C}_2H_5 (+M) \rightarrow C_2H_4 + \dot{H} (+M)$, $C_2H_6 + \dot{H} \rightarrow \dot{C}_2H_5 + H_2$, ... develops, consuming the fuel and producing H atoms. Therefore, ethane is mainly consumed by H-atom abstraction by H atoms. From these studies, we observe that as time progresses, reactions involving the secondary radicals formed in the system also become important, in addition to the unimolecular dissociation reactions. Figure 9(b) presents a sensitivity analysis for the aforementioned fuels at their threshold temperatures and reveals that the fuel decomposition reactions are consistently one of the most sensitive reactions for all cases despite their limited contribution to fuel consumption. For methane, the sensitivity towards the $CH_4 (+M) \leftrightarrow \dot{C}H_3 + \dot{H} (+M)$ reaction is almost nine times larger than that for H-atom abstraction by H atoms and $\dot{C}H_3$ radicals. This high sensitivity of UMD reactions is primarily attributed to the reaction kinetics in the early phase of the pyrolysis process. In Fig. 6(a), the dashed lines indicate the contribution of the UMD reactions as a function of time for *n*- C_5H_{12} consumption. It can be observed that the UMD reactions solely initiate *n*-pentane consumption leading to the production of key radicals which then proceed to undergo H-atom abstraction from the fuel. As these secondary reactions become dominant ($> 1 \times 10^4$ s) the role of UMD reactions diminish ($< 10\%$). Therefore, since the UMD initiate fuel consumption even

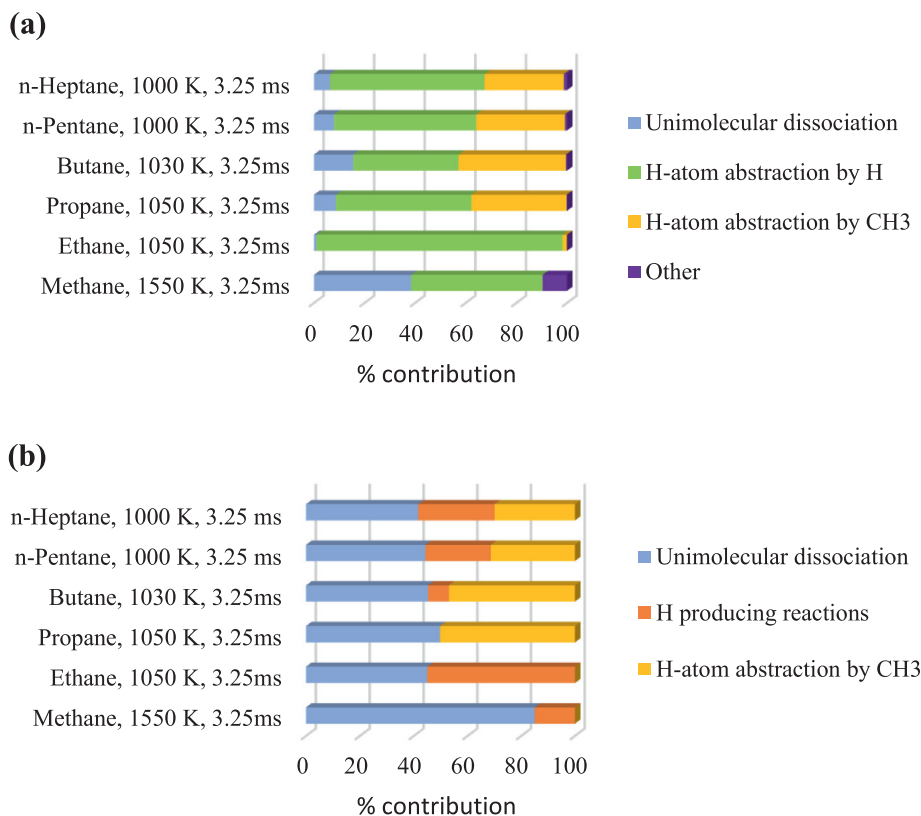


Fig. 9. (a) Integrated fuel consumption flux through various reaction channels for alkanes. (b) Relative sensitivities towards fuel concentration of different reaction classes. All the calculations were performed at T_{thres} , $p = 2$ bar, $\tau_{res} = 3.25$ ms for alkanes.

though they have a low contribution to overall fuel consumption, they show large sensitivity coefficients.

For alkanes with three or more carbon atoms, H-atom abstraction by $\dot{C}H_3$ radicals are the second most important reactions followed by reactions involving \dot{H} atom additions and abstractions. This trend indicates that fuel decomposition reaction rates play a major role in controlling the initiation temperature of fuel pyrolysis, corroborating our discussion in Section 3.2 above.

3.3.2. Analysis of alkene pyrolysis

In the case of alkenes, there is a possibility of \dot{H} atom and $\dot{C}H_3$ radical addition to the vinylic carbon sites and this contributes to fuel consumption. Due to the disparate fuel consumption pathways, the reactivities of different fuels are different. This is explored further by comparing the reactivities of ethylene (C_2H_4), propene (C_3H_6), 1-butene ($1-C_4H_8$), isobutene ($i-C_4H_8$), 1-pentene ($1-C_5H_{10}$), 2-methyl-1-butene (aC_5H_{10} , 2M1B) and 3-methyl-1-butene (cC_5H_{10} , 3M1B). An integrated fuel consumption flux analysis is performed at their respective threshold temperatures, Fig. 10. The reaction time is 3.25 ms for all cases shown.

It is observed that the radicals formed from unimolecular dissociation control the subsequent secondary pathways. Even though the contribution of UMD towards fuel consumption is less than 20%, its importance is seen in our sensitivity analysis, Fig. 10(b). Furthermore, in alkanes, \dot{H} atoms are consumed by abstraction reactions producing molecular hydrogen whereas in alkenes, \dot{H} addition reactions are dominant and produce a smaller olefin and a radical, see Figs. 9(a) and 10(a). Moreover, other reactions such as retro-ene, \dot{H} atom addition and $\dot{C}H_3$ addition also contribute to fuel consumption. Clearly, UMD is important in initiating pyrolysis and hence, these reactions are sensitive. A further analysis is performed by comparing propene and isobutene. Propene and isobutene have similar unimolecular dissociation rate con-

stants and hence, their pyrolytic initiation is similar at 2 bar (Fig. 11). However, once the initial radical pool is formed, the rates of H-atom abstraction by methyl radicals are higher for isobutene due to the relatively higher concentration of methyl radicals produced, mainly from the β -scission of 2-methyl allyl (iC_4H_7) radicals. Therefore, isobutene is highly sensitive to the rate constant for the reaction $iC_4H_7 \rightarrow C_3H_4 + \dot{C}H_3$. Rate of production analyses for 2% propene and isobutene at 1300 K and 2 bar are illustrated in Fig. 12. Methyl assisted abstraction dominates isobutene consumption but the \dot{H} atom assisted chemically activated pathway is the major consumption pathway for propene (Fig. 13). Hence, the propene mole fraction is mainly sensitive to UMD reactions producing \dot{H} atoms and the isobutene mole fraction is sensitive to both UMD and the β -scission of iC_4H_7 radicals. Clearly, UMD reactions establish the reaction pathways for both propene and isobutene.

In the case of ethylene, UMD of ethylene produces vinyl (\dot{C}_2H_3) radicals and \dot{H} atoms, with \dot{C}_2H_3 radicals decomposing to form acetylene (C_2H_2) + \dot{H} . Also, the 1,1-elimination reaction of ethylene to form a carbene is one to two order of magnitude faster than the UMD depending on the temperature. The \dot{H} atoms produced abstract H-atoms from ethylene creating a self-sustaining loop, $C_2H_4 + \dot{H} \rightarrow \dot{C}_2H_3 + H_2$ and $\dot{C}_2H_3 (+M) \rightarrow C_2H_2 + \dot{H} (+M)$, $C_2H_4 + \dot{H} \rightarrow \dot{C}_2H_3 + H_2$, ... (similar to ethane for alkanes above) consuming the fuel and producing H_2 , C_2H_2 and \dot{H} atoms. Therefore, the ethylene mole fraction is sensitive to the rate constants for UMD, H-atom abstraction by \dot{H} and β -scission of vinyl radicals. Due to the difficulty of cleaving a vinylic C-H bond, ethylene is the slowest to decompose among all of the alkenes.

1-Butene and 2M1B undergo UMD to produce resonantly stabilized radicals, \dot{C}_3H_5 -a for 1-butene and 1,3- \dot{C}_4H_7 for 2M1B in addition to a $\dot{C}H_3$ radical. Hence, the fuel is consumed mainly by H-atom abstraction by $\dot{C}H_3$ radicals. Both \dot{C}_3H_5 -a and 1,3-

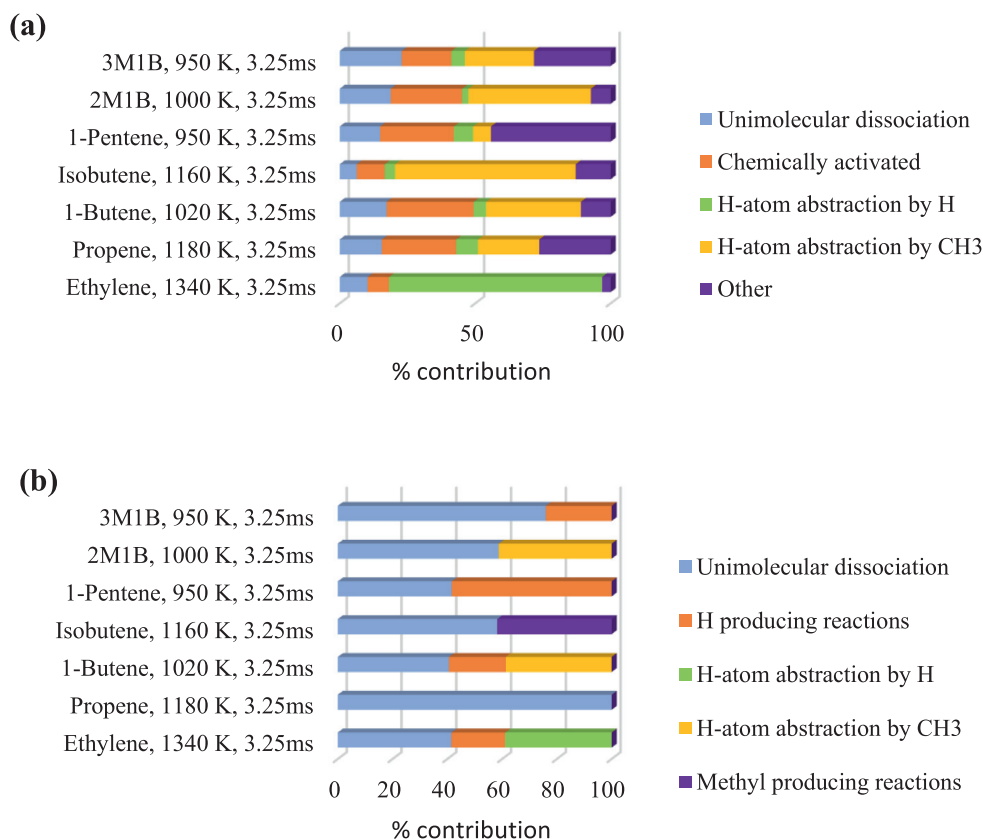


Fig. 10. (a) Integrated fuel consumption flux through various reaction channels for alkenes. (b) Relative sensitivities towards fuel concentration of different reaction classes at T_{thres} , $p = 2$ bar, $\tau_{res} = 3.25$ ms for alkenes.

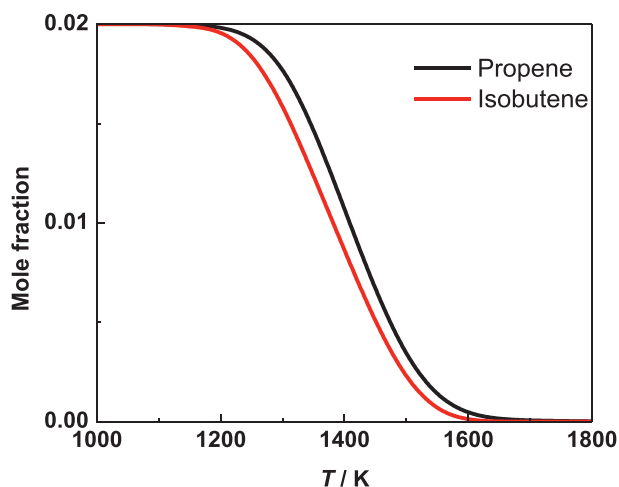


Fig. 11. 2% propene and isobutene pyrolysis at 2 bar.

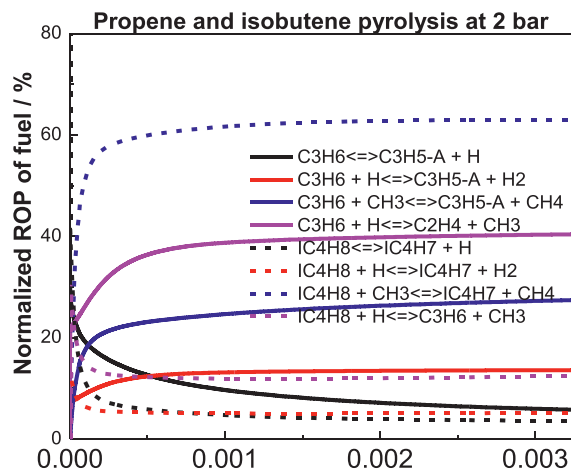


Fig. 12. Normalized fuel ROP analyses for 2% propene and isobutene at 1300 K and 2 bar.

\dot{C}_4H_7 radicals produce \dot{H} atoms via β -scission. Therefore, \dot{H} atom assisted reactions also contribute to the consumption of these fuels. Similarly, in the case of 2M1B, H-atom abstraction produces 2-methyl-1-buten-3-yl radicals ($\dot{a}C_5H_9-c$), which also undergo β -scission producing \dot{H} atoms which contribute to fuel consumption.

From the above analyses, we see that in the case of alkanes, UMD and H-atom abstraction reactions are the key reaction pathways consuming the fuel under pyrolytic conditions. Alkenes have similar reaction pathways but are also consumed by chemically activated pathways which essentially convert a larger olefin into a smaller olefin and a smaller radical, e.g. $C_3H_6 + \dot{H} \leftrightarrow C_2H_4 + \dot{C}H_3$.

3.4. Limiting normalized progress of reaction factor

In this section, we extend our investigation to determine the effect of initial partial pressure of the fuel and reaction residence time on T_{thres} . Table 3 lists the T_{thres} determined for the various alkanes and alkenes through numerical simulations and it clearly shows that the T_{thres} is significantly dependent on these factors. Higher residence times and higher fuel partial pressures lead to faster pyrolysis with respect to temperature, thus resulting in a lower T_{thres} for each fuel. For example, for CH_4 the T_{thres} lowers by ~ 70 K when the fuel partial pressure is increased from 0.04

Table 3
Limiting rates for different fuels at their threshold temperatures.

Fuel	p (bar)	Residence time τ_{res} (s)	Fuel mole fraction	T_{thres} (K)	$RR_{sum}(\text{UMD} + \dot{H} \text{ abst. by } \dot{H} + \dot{H} \text{ abst. by } \text{CH}_3 + \text{chemically activated})(\text{mol cm}^{-3} \text{ s}^{-1})$	NormalizedPRF ($RR_{sum}^* \tau_{res}/p_{fuel}$), ($\text{mol cm}^{-3} \text{ bar}^{-1}$)	
CH ₄	2	3.25×10^{-3}	0.02	1560	1.06×10^{-6}	8.61×10^{-8}	
	2	0.10	0.02	1380	2.43×10^{-8}	6.08×10^{-8}	
	10	3.25×10^{-3}	0.05	1490	9.19×10^{-6}	5.97×10^{-8}	
	2	10	0.02	1220	3.20×10^{-10}	7.99×10^{-8}	
	2	$1.80 \times 10^{+3}$	0.02	1060	1.60×10^{-6}	7.28×10^{-8}	
	1	$1.80 \times 10^{+3}$	0.02	1070	7.28×10^{-13}	6.56×10^{-8}	
	20	$1.80 \times 10^{+3}$	0.02	1025	6.77×10^{-12}	3.03×10^{-8}	
	20	$1.80 \times 10^{+3}$	0.10	1005	1.52×10^{-11}	1.37×10^{-8}	
	5	1	0.02	1275	5.77×10^{-9}	5.77×10^{-8}	
	C ₃ H ₈	2	3.25×10^{-3}	0.02	1075	1.29×10^{-6}	1.05×10^{-7}
2		0.10	0.02	960	4.42×10^{-8}	1.11×10^{-7}	
10		3.25×10^{-3}	0.05	1010	7.00×10^{-6}	4.55×10^{-8}	
2		10	0.02	825	3.17×10^{-10}	7.93×10^{-8}	
2		$1.80 \times 10^{+3}$	0.02	725	1.68×10^{-12}	7.57×10^{-8}	
1		$1.80 \times 10^{+3}$	0.02	720	5.81×10^{-13}	5.38×10^{-8}	
20		$1.80 \times 10^{+3}$	0.02	725	1.86×10^{-11}	8.37×10^{-8}	
20		$1.80 \times 10^{+3}$	0.10	710	4.22×10^{-11}	3.82×10^{-8}	
5		1	0.02	865	5.77×10^{-9}	5.77×10^{-8}	
1		100	0.1	775	6.64×10^{-11}	6.64×10^{-8}	
0.4		0.01	0.05	1040	1.61×10^{-7}	8.05×10^{-8}	
10		0.01	0.1	980	5.73×10^{-6}	5.73×10^{-8}	
10		100	0.1	760	4.24×10^{-10}	4.24×10^{-8}	
n-C ₄ H ₁₀		2	3.25×10^{-3}	0.02	1030	5.77×10^{-7}	4.69×10^{-8}
		2	0.10	0.02	920	3.76×10^{-8}	9.40×10^{-8}
	20	$1.80 \times 10^{+3}$	0.10	675	3.9×10^{-11}	3.51×10^{-8}	
	10	1	0.01	845	6.29×10^{-9}	6.29×10^{-8}	
	10	0.01	0.1	950	5.50×10^{-6}	5.50×10^{-8}	
	0.4	0.01	0.05	975	8.85×10^{-8}	4.42×10^{-8}	
	10	100	0.1	730	5.54×10^{-10}	5.54×10^{-8}	
	i-C ₄ H ₁₀	2	3.25×10^{-3}	0.02	1005	1.53×10^{-6}	1.24×10^{-7}
2		0.10	0.02	890	4.00×10^{-8}	1.00×10^{-7}	
20		$1.80 \times 10^{+3}$	0.10	705	2.99×10^{-11}	2.69×10^{-8}	
n-C ₅ H ₁₂	2	3.25×10^{-3}	0.02	1000	9.83×10^{-7}	7.99×10^{-8}	
	2	0.10	0.02	890	1.68×10^{-8}	4.20×10^{-8}	
	2	10	0.02	805	1.61×10^{-10}	4.04×10^{-8}	
	2	$1.80 \times 10^{+3}$	0.02	740	1.44×10^{-12}	6.50×10^{-8}	
	1	$1.80 \times 10^{+3}$	0.02	745	5.78×10^{-13}	5.20×10^{-8}	
	20	$1.80 \times 10^{+3}$	0.02	730	7.96×10^{-11}	3.58×10^{-8}	
	20	$1.80 \times 10^{+3}$	0.10	725	2.76×10^{-11}	2.48×10^{-8}	
	10	1	0.01	850	6.17×10^{-9}	6.14×10^{-8}	
	10	0.01	0.1	950	5.00×10^{-6}	5.00×10^{-8}	
	10	100	0.1	775	4.02×10^{-10}	4.02×10^{-8}	
	0.4	0.01	0.05	975	1.24×10^{-7}	6.20×10^{-8}	
	1	100	0.1	775	3.70×10^{-11}	3.70×10^{-8}	
	i-C ₅ H ₁₂	2	3.25×10^{-3}	0.02	1000	8.46×10^{-7}	6.87×10^{-8}
		2	0.10	0.02	900	2.73×10^{-8}	6.83×10^{-8}
		20	$1.80 \times 10^{+3}$	0.10	725	5.16×10^{-11}	4.64×10^{-8}
neoC ₅ H ₁₂	2	3.25×10^{-3}	0.02	1030	9.78×10^{-7}	7.95×10^{-8}	
	2	0.10	0.02	930	3.27×10^{-8}	8.18×10^{-8}	
	10	3.25×10^{-3}	0.05	990	7.92×10^{-6}	5.15×10^{-8}	
	2	3.25×10^{-3}	0.02	995	9.23×10^{-7}	7.50×10^{-8}	
	2	0.10	0.02	890	2.70×10^{-8}	6.75×10^{-8}	
	20	$1.80 \times 10^{+3}$	0.10	730	5.03×10^{-11}	4.53×10^{-8}	
2,3-DMB	2	3.25×10^{-3}	0.02	960	7.70×10^{-7}	6.26×10^{-8}	
	2	0.10	0.02	870	2.73×10^{-8}	6.83×10^{-8}	
n-C ₇ H ₁₆	2	3.25×10^{-3}	0.02	995	1.21×10^{-6}	9.83×10^{-8}	
	2	0.10	0.02	890	2.14×10^{-8}	5.35×10^{-8}	
	2	10	0.02	800	1.87×10^{-10}	4.66×10^{-8}	
	2	$1.80 \times 10^{+3}$	0.02	705	6.30×10^{-13}	2.83×10^{-8}	
	1	$1.80 \times 10^{+3}$	0.02	715	3.89×10^{-13}	3.51×10^{-8}	
	20	$1.80 \times 10^{+3}$	0.02	715	9.09×10^{-12}	4.09×10^{-8}	
	20	$1.80 \times 10^{+3}$	0.10	695	1.42×10^{-11}	1.28×10^{-7}	
	10	0.01	0.1	940	4.34×10^{-6}	4.34×10^{-8}	
	0.4	0.01	0.05	950	9.01×10^{-8}	4.50×10^{-8}	
	1	100	0.1	760	4.74×10^{-11}	4.74×10^{-8}	
C ₃ H ₆	10	100	0.1	735	5.50×10^{-10}	5.50×10^{-8}	
	2	3.25×10^{-3}	0.02	1180	4.16×10^{-7}	3.38×10^{-8}	
	2	0.01	0.02	1160	2.79×10^{-7}	6.97×10^{-8}	
	10	1	0.01	1025	8.49×10^{-9}	8.49×10^{-8}	
	10	0.01	0.1	1145	6.06×10^{-6}	6.06×10^{-8}	
	0.4	0.01	0.05	1175	1.50×10^{-7}	7.50×10^{-8}	

(continued on next page)

Table 3 (continued)

Fuel	p (bar)	Residence time τ_{res} (s)	Fuel mole fraction	T_{thres} (K)	$RR_{sum}(UMD + \dot{H}$ abst. by $\dot{H} + \dot{H}$ abst. by $\dot{C}H_3 +$ chemically activated)(mol cm ⁻³ s ⁻¹)	NormalizedPRF ($RR_{sum} * \tau_{res}/p_{fuel}$)(mol cm ⁻³ bar ⁻¹)	
1-C ₄ H ₈	2	3.25 × 10 ⁻³	0.02	1020	1.58 × 10 ⁻⁶	1.29 × 10 ⁻⁷	
	2	0.01	0.02	980	4.73 × 10 ⁻⁷	1.18 × 10 ⁻⁷	
	2	0.10	0.02	900	2.75 × 10 ⁻⁸	6.88 × 10 ⁻⁸	
	20	1.8 × 10 ⁺³	0.1	710	8.31 × 10 ⁻¹¹	8.61 × 10 ⁻⁸	
	20	10	0.1	800	1.78 × 10 ⁻⁸	8.90 × 10 ⁻⁸	
	10	0.01	0.1	945	7.48 × 10 ⁻⁶	7.48 × 10 ⁻⁸	
	20	10	0.02	800	3.78 × 10 ⁻⁹	9.45 × 10 ⁻⁸	
	10	1	0.01	825	3.37 × 10 ⁻⁹	3.37 × 10 ⁻⁸	
	10	100	0.1	755	7.16 × 10 ⁻¹⁰	7.16 × 10 ⁻⁸	
	0.4	0.01	0.05	975	1.78 × 10 ⁻⁷	8.90 × 10 ⁻⁸	
	1	100	0.1	760	1.09 × 10 ⁻¹⁰	1.09 × 10 ⁻⁷	
	i-C ₄ H ₈	2	3.25 × 10 ⁻³	0.02	1160	6.15 × 10 ⁻⁷	5.00 × 10 ⁻⁸
		2	0.10	0.02	1050	1.85 × 10 ⁻⁸	4.62 × 10 ⁻⁸
20		1.8 × 10 ⁺³	0.1	870	9.20 × 10 ⁻¹¹	8.28 × 10 ⁻⁸	
20		10	0.1	970	1.34 × 10 ⁻⁸	6.70 × 10 ⁻⁸	
20		10	0.02	970	5.04 × 10 ⁻⁹	1.26 × 10 ⁻⁷	
0.4		0.01	0.05	1150	2.30 × 10 ⁻⁷	1.15 × 10 ⁻⁷	
10		1	0.01	1000	7.40 × 10 ⁻⁷	7.40 × 10 ⁻⁸	
10		0.01	0.1	1125	4.98 × 10 ⁻⁶	4.98 × 10 ⁻⁸	
10		100	0.1	925	8.50 × 10 ⁻¹⁰	8.50 × 10 ⁻⁸	
1		100	0.1	910	6.46 × 10 ⁻¹¹	6.46 × 10 ⁻⁸	
1-C ₅ H ₁₀		2	3.25 × 10 ⁻³	0.02	950	5.39 × 10 ⁻⁷	4.38 × 10 ⁻⁸
		20	1.8 × 10 ⁺³	0.1	675	1.10 × 10 ⁻¹⁰	9.92 × 10 ⁻⁸
		20	10	0.1	750	1.16 × 10 ⁻⁸	5.78 × 10 ⁻⁸
	10	0.01	0.1	925	7.22 × 10 ⁻⁶	7.22 × 10 ⁻⁸	
	10	1	0.01	820	1.14 × 10 ⁻⁸	1.14 × 10 ⁻⁷	
	0.4	0.01	0.05	925	1.61 × 10 ⁻⁷	8.05 × 10 ⁻⁸	
	10	100	0.1	710	3.50 × 10 ⁻¹⁰	3.50 × 10 ⁻⁸	
	20	10	0.02	770	3.80 × 10 ⁻⁹	9.50 × 10 ⁻⁸	
	aC ₅ H ₁₀	2	3.25 × 10 ⁻³	0.02	1000	8.33 × 10 ⁻⁷	6.77 × 10 ⁻⁸
		20	1.8 × 10 ⁺³	0.1	725	1.11 × 10 ⁻¹⁰	9.99 × 10 ⁻⁸
		20	10	0.1	810	1.64 × 10 ⁻⁸	8.19 × 10 ⁻⁸
		20	10	0.02	810	3.20 × 10 ⁻⁹	8.00 × 10 ⁻⁸
		10	1	0.01	850	7.69 × 10 ⁻⁹	7.69 × 10 ⁻⁸
0.4		0.01	0.05	975	1.89 × 10 ⁻⁷	9.45 × 10 ⁻⁸	
10		100	0.1	760	1.04 × 10 ⁻⁹	1.04 × 10 ⁻⁷	
1		100	0.1	760	1.10 × 10 ⁻¹⁰	1.10 × 10 ⁻⁷	
bC ₅ H ₁₀		2	3.25 × 10 ⁻³	0.02	1080	7.99 × 10 ⁻⁷	6.49 × 10 ⁻⁸
		20	1.8 × 10 ⁺³	0.1	800	1.21 × 10 ⁻¹⁰	1.09 × 10 ⁻⁷
		20	10	0.1	890	8.93 × 10 ⁻⁹	4.47 × 10 ⁻⁸
		10	1	0.01	950	8.13 × 10 ⁻⁹	8.13 × 10 ⁻⁸
		10	100	0.1	850	8.41 × 10 ⁻¹⁰	8.41 × 10 ⁻⁸
	20	10	0.02	895	2.75 × 10 ⁻⁹	6.88 × 10 ⁻⁸	
	10	0.01	0.1	1080	8.82 × 10 ⁻⁶	8.82 × 10 ⁻⁸	
	0.4	0.01	0.05	1095	2.17 × 10 ⁻⁷	1.05 × 10 ⁻⁷	
	1	100	0.1	840	4.00 × 10 ⁻¹¹	4.00 × 10 ⁻⁸	
	cC ₅ H ₁₀	10	3.25 × 10 ⁻³	0.02	1080	4.12 × 10 ⁻⁶	6.70 × 10 ⁻⁸
		2	3.25 × 10 ⁻³	0.02	950	7.43 × 10 ⁻⁷	6.04 × 10 ⁻⁸
		20	1.8 × 10 ⁺³	0.1	690	8.61 × 10 ⁻¹¹	7.75 × 10 ⁻⁸
		20	10	0.1	775	1.88 × 10 ⁻⁸	9.40 × 10 ⁻⁸
10		1	0.01	820	1.01 × 10 ⁻⁸	1.01 × 10 ⁻⁷	
10		0.01	0.1	925	1.07 × 10 ⁻⁵	1.07 × 10 ⁻⁷	
0.4		0.01	0.05	930	2.26 × 10 ⁻⁷	1.10 × 10 ⁻⁷	
10		100	0.1	735	8.89 × 10 ⁻¹⁰	8.89 × 10 ⁻⁸	
1		100	0.1	740	1.24 × 10 ⁻¹⁰	1.24 × 10 ⁻⁷	
20		10	0.02	775	3.83 × 10 ⁻⁰⁹	9.58 × 10 ⁻⁸	

to 0.5 bar for a residence time of 3.25 ms. Similarly, the T_{thres} reduces by ~180 K when the residence time is increased from 3.25 to 100 ms while maintaining the same initial fuel partial pressure for CH₄.

In an attempt to determine a parameter for characterizing fuel pyrolysis initiation irrespective of the residence time or the fuel partial pressure, we propose a normalized 'progress of reaction factor' (PRF) here. The normalized PRF is calculated by summing the rates of key reactions involved in fuel consumption (Section 3.3) at the end of residence time, multiplied by the τ_{res} and normalized with respect to the fuel partial pressure as shown in the equation:

$$PRF = \left(\sum RR_{UMD} + \sum RR_{H-abst} + \dots \right) * \tau_{res} / P_{Fuel} \quad (1)$$

Table 3 provides the normalized PRF values for fuel pyrolysis under different conditions (τ_{res} and fuel partial pressures) at their corresponding threshold temperatures. The operating conditions considered for this analysis span over residence times of 3.25 ms – 30 min (~5 orders of magnitude) and fuel partial pressures of 0.02 – 2.0 bar (~2 orders of magnitude). It should be noted that a mean normalized limiting PRF value of $\sim 7.06 \times 10^{-8}$ mol cm⁻³ bar⁻¹ is observed with an overall standard deviation of only ~36% for this wide array of fuels and conditions. Figure 14 compares the deviations in the PRF value for each test condition along with the total reaction rate of the key reactions (UMD + \dot{H} abst. by $\dot{H} + \dot{H}$ abst. by $\dot{C}H_3 +$ chemically activated). This clearly shows that while the chemical timescales tend to vary significantly (~7 orders of mag-

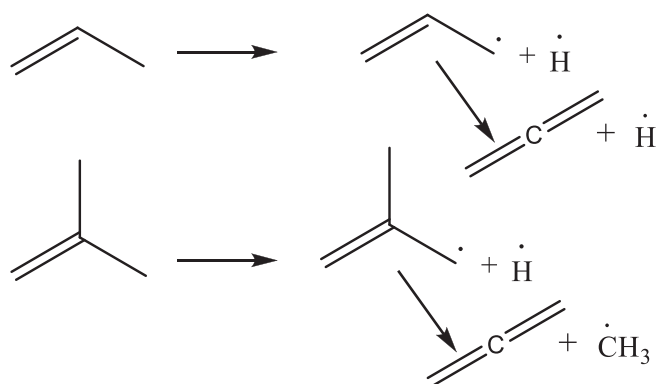


Fig. 13. Propene and isobutene initiation pathways.

nitude), the standard deviation in the normalized PRF values is only ~36% over the range of partial pressure (0.02 – 2.0 bar), residence time (3 ms – 30 min) and the type of fuel (alkanes, alkenes and their isomers). Additional plots showing variation in PRF as a function of residence time and fuel partial pressure are provided as Supplementary material. The figures show that PRF values typically lie within a similar range of values. Even though the fuels have different geometrical structures and thermodynamic properties, they begin to pyrolyze only when their PRF is greater than the limiting PRF. This unique limiting PRF value represents an effective amount of fuel necessary to be consumed in a given time for an observable pyrolysis process. This value could thus help to determine the threshold temperature for a given fuel concentration, pressure and residence time. To the best of our knowledge, this is the first study to provide a unique limiting factor for the pyrolysis process for the alkanes and alkenes included here. Furthermore, the concept of threshold temperature is introduced in this study and its dependence on UMD reaction rate constants is clearly shown.

An in-house Python program [20] based on Goodwin et al. [21] is developed to provide the PRF at any given condition for a number of fuels and is provided as Supplementary material. This

program can be used to predict the initiation of pyrolysis for any fuel. A step-by-step process on understanding the pyrolysis of alkanes and alkenes culminated in this program. This novel approach provided in the current study can aid researchers to further explore pyrolysis, as it is one of the important chemical transformation processes. Heating rate, temperature, pressure and residence time are vital control parameters [2,3]. Through a proper choice of residence time and pyrolysis temperature, the yield can be controlled and optimized.

To determine the minimum temperature at which the conversion begins for a given residence time and pressure, the concept of PRF can be utilized. Industrial scale pyrolysis is part of several of the most important industrial activities including the processing of oil, natural gas, coal, and different types of waste [22] and the concept of PRF and threshold temperature has applications in this domain.

3.5. Application of threshold temperature in fundamental studies

0-D constant volume simulations were performed at 800 K and 1200 K at 1 bar pressure and equivalence ratio (φ) of 1 to show the application of threshold temperature.

In the former case ignition delay time (IDT) is determined to be 4.85 s and using this as residence time, we obtain the corresponding T_{thres} as 850 K. Since the reaction temperature is below the T_{thres} , chain initiation is led by the abstraction reactions and this is corroborated by Fig. 15(a). Abstraction reactions are observed to be the major fuel consumption pathways at 0.1% fuel consumption. In contrast, at 1200 K when the IDT is 8 ms and the T_{thres} is 1100 K, it is observed that the UMD reaction is the most important fuel consumption reaction at 0.1% fuel consumption, Fig. 15(b). When a brute force sensitivity analysis for IDT is performed for these two cases, we do not see sensitivity of UMD reactions of the fuel when the reaction temperature is below T_{thres} , Fig. 15(c) and (d).

Our analysis was further extended to 1-butene. In Fig. 16(a), the reaction temperature is below the T_{thres} (850 K). Hence, we do not observe sensitivity of fuel pyrolysis reactions to IDT predictions. Moreover, initiation occurs via the fuel + O_2 reaction. How-

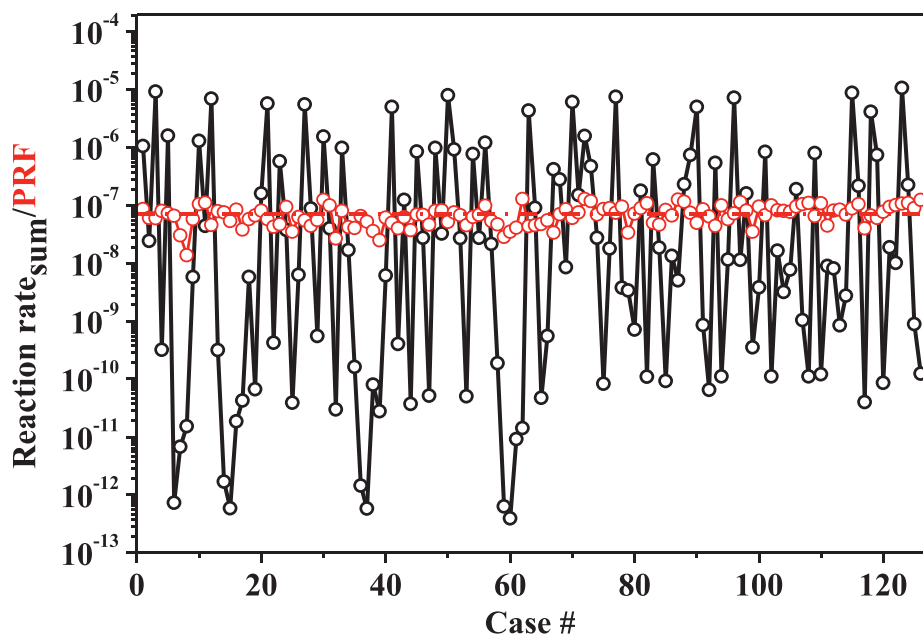


Fig. 14. Comparison of the reaction rate (black) and the 'Progress of Reaction Factor' (red) for different fuels at residence time and fuel partial pressure ranging from 3 ms to 30 min and 0.02 – 2 bar, respectively. Detailed conditions are listed in Table 3. (For interpretation of the references to color in this figure legend, the reader is referred to the web version of this article.)

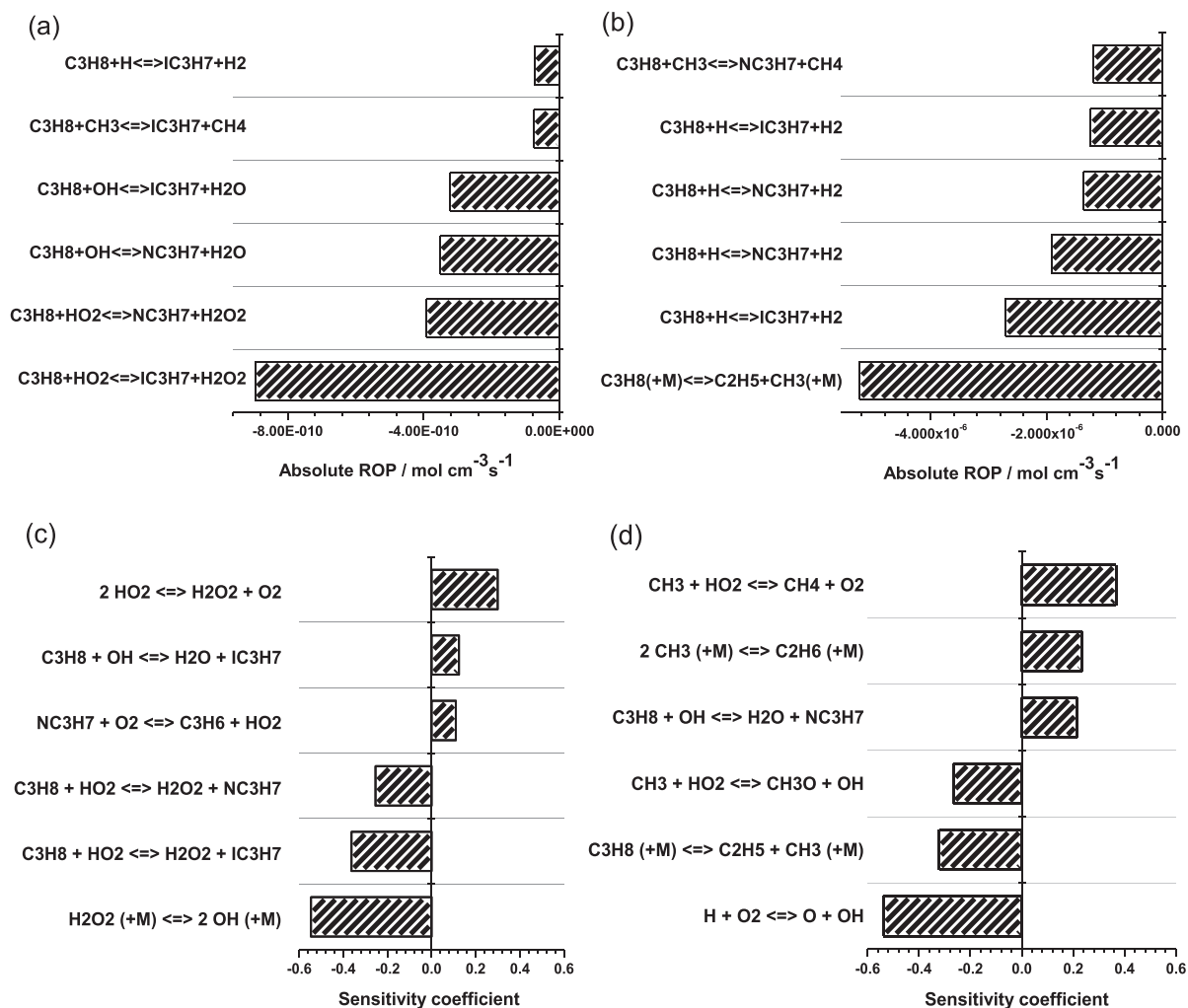


Fig. 15. (a) Propane ROP analysis 0.1% fuel consumption, $\phi = 1$, 1 bar and 800 K. (b) Propane ROP analysis 0.1% fuel consumption, $\phi = 1$, 1 bar and 1200 K. (c) Brute force sensitivity analysis for propane IDT in air at 1 bar, $\phi = 1$ and 800 K. (d) Brute force sensitivity analysis for propane IDT in air at 1 bar, $\phi = 1$ and 1200 K.

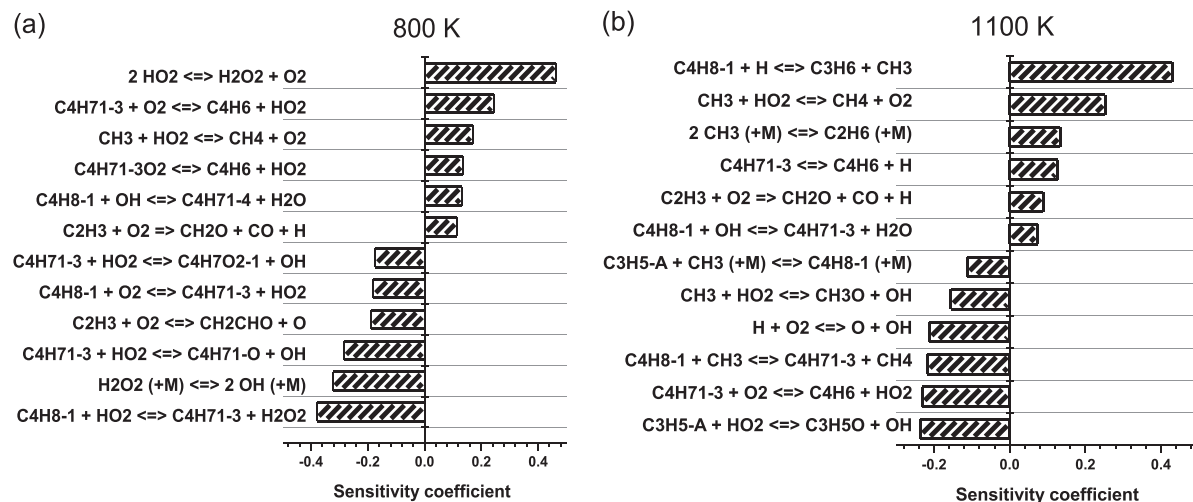


Fig. 16. Sensitivity analysis for 1-butene IDT at 1 bar, $\phi = 1$ and (a) 800 K; (b) 1100 K.

ever, in Fig. 16(b), the reaction temperature is above the T_{thres} of 980 K. Therefore, we observe that initiation occurs via UMD of the fuel and subsequently, the IDT is sensitive to fuel UMD and H-atom abstraction by $\dot{C}H_3$ radicals and chemical activation by H atoms. Based on these four cases with the two fuels, it is deter-

mined that in a shock tube at $T > 1000$ K and τ_{res} in the μ s–ms timescale, the reaction temperature is usually higher than the threshold temperature under these conditions and hence, chain initiation happens via UMD and hence IDTs are sensitive to UMD reactions.

In contrast, if the reaction temperature is below T_{thres} for a given pressure and τ_{res} , which is usually the case for jet-stirred reactor and flow reactor studies, chain initiation occurs via H-atom abstraction from the fuel by O_2 . Therefore, in these reactors fuel reactivity is not usually observed to be sensitive to UMD reactions.

4. Conclusions

Simulation of the pyrolysis of $C_1 - C_7$ hydrocarbons have been performed using NUIGMech1.1 at a constant initial fuel concentration, pressure, and reaction time in the temperature range of 900 – 2000 K. It is observed that the products of unimolecular dissociation determine the secondary fuel consumption pathways. Hence, fuel pyrolysis is highly sensitive to unimolecular dissociation reactions. We found anomalies with ethane and ethylene, where on H-atom abstraction the ethyl (in ethane) and vinyl (in ethylene) radicals decompose to form $C_2H_4 + \dot{H}$ and $C_2H_2 + \dot{H}$ respectively. This is followed by a cycle of $C_2H_6/C_2H_4 + \dot{H} = \dot{C}_2H_5/\dot{C}_2H_3 + H_2$, and $\dot{C}_2H_5/\dot{C}_2H_3 = C_2H_4/C_2H_2 + \dot{H}$, $C_2H_6/C_2H_4 + \dot{H}...$

Furthermore, fuel consumption is noticeable only when the progress of reaction factor (PRF) is $\geq 7.06 \times 10^{-8} \pm 36\% \text{ mol cm}^{-3} \text{ bar}^{-1}$. A computer program is developed based on this limiting PRF approach and is a tool for the user to determine the threshold temperature for the pyrolysis of a fuel. It is shown that because of (i) the net zero effect of H-atom abstraction by $\dot{C}H_3$ radicals, (ii) the relatively higher BDE for cleavage of C–H bond compared to a C–C bond, and (iii) the quasi equilibrium established in the intermediate phase ($\tau = 10^{-7} - 10^{-5} \text{ s}$), methane is slower to decompose relative to all of the other fuels. Moreover, ethylene shows the lowest reactivity among the alkenes due to the higher BDE of vinylic C–H bonds. Furthermore, even though the UMD rate constants of propene and isobutene are similar, the secondary reactions of these two fuels lead to different overall reactivity, illustrating the importance of the secondary reactions. Finally, the existence of a limiting threshold temperature and its influence on chain initiation and IDT sensitivity is illustrated.

Declaration of Competing Interest

None

Acknowledgments

The authors would like to acknowledge Science Foundation Ireland for funding via project numbers 15/IA/3177 and 16/SP/3829. The authors would also acknowledge Dr. Charles Westbrook and Prof. Karl Alexander Heufer for fruitful discussions during manuscript preparation.

Supplementary materials

Supplementary material associated with this article can be found, in the online version, at doi:10.1016/j.combustflame.2021.111579.

References

- [1] K. Rajendran, R. Lin, D.M. Wall, J.D. Murphy, Influential aspects in waste management practices, *Sustain. Resour. Recover. Zero Waste Approaches* (2019), doi:10.1016/B978-0-444-64200-4.00005-0.
- [2] P. Basu, Biomass gasification, pyrolysis and torrefaction: practical design and theory, 2018. 10.1016/C2016-0-04056-1.
- [3] F.X. Collard, M. Carrier, J.F. Görgens, Fractionation of lignocellulosic material with pyrolysis processing, *Biomass Fract. Technol. Lignocellul. Feed Based Biorefin.* (2016), doi:10.1016/B978-0-12-802323-5.00004-9.
- [4] A.V. Bridgwater, Review of fast pyrolysis of biomass and product upgrading, *Biomass Bioenergy* 38 (2012) 68–94, doi:10.1016/j.biombioe.2011.01.048.
- [5] S.S. Nagaraja, J. Liang, S. Dong, S. Panigrahy, A. Sahu, G. Kukkadapu, S.W. Wagnon, W.J. Pitz, H.J. Curran, A hierarchical single-pulse shock tube pyrolysis study of C2 – C6 1-alkenes, *Combust. Flame*. 219 (2020) 456–466.
- [6] S.S. Nagaraja, J. Power, G. Kukkadapu, S. Dong, S.W. Wagnon, W.J. Pitz, H.J. Curran, A single pulse shock tube study of pentene isomer pyrolysis, *Proc. Combust. Inst.* 38 (2020) 881–889, doi:10.1016/j.proci.2020.06.069.
- [7] S.S. Nagaraja, G. Kukkadapu, S. Panigrahy, J. Liang, H. Lu, W.J. Pitz, H.J. Curran, A pyrolysis study of allylic hydrocarbon fuels, *Int. J. Chem. Kinet.* 52 (2020) 964–978.
- [8] D. Nativel, B. Shu, J. Herzler, M. Fikri, C. Schulz, Shock-tube study of methane pyrolysis in the context of energy-storage processes, *Proc. Combust. Inst.* 37 (2019) 197–204, doi:10.1016/j.proci.2018.06.083.
- [9] Y. Hidaka, S. Shiba, H. Takuma, M. Suga, Thermal decomposition of ethane in shock waves, *Int. J. Chem. Kinet.* 17 (1985) 441–453, doi:10.1002/kin.550170410.
- [10] Y. Hidaka, T. Oki, H. Kawano, Thermal decomposition of propane in shock waves, *Int. J. Chem. Kinet.* 21 (1989) 689–701, doi:10.1002/kin.550210808.
- [11] K. Yasunaga, H. Yamada, H. Oshita, K. Hattori, Y. Hidaka, H. Curran, Pyrolysis of *n*-pentane, *n*-hexane and *n*-heptane in a single pulse shock tube, *Combust. Flame* 185 (2017) 335–345.
- [12] J.N. Bradley, K.O. West, Single-pulse shock tube studies of hydrocarbon pyrolysis: part 5. Pyrolysis of neopentane, *J. Chem. Soc. Faraday Trans. 1 Phys. Chem. Condens. Phases* 72 (1976) 558–567, doi:10.1039/F19767200008.
- [13] T. Malewicki, A. Comandini, K. Brezinsky, Experimental and modeling study on the pyrolysis and oxidation of ISO-octane, *Proc. Combust. Inst.* 34 (2013) 353–360, doi:10.1016/j.proci.2012.06.137.
- [14] T. Malewicki, K. Brezinsky, Experimental and modeling study on the pyrolysis and oxidation of *n*-decane and *n*-dodecane, *Proc. Combust. Inst.* 34 (2013) 361–368, doi:10.1016/j.proci.2012.06.156.
- [15] S. Dooley, H.J. Curran, J.M. Simmie, Autoignition measurements and a validated kinetic model for the biodiesel surrogate, methyl butanoate, *Combust. Flame* 153 (2008) 2–32.
- [16] R. CHEMKIN-PRO, 15112, Reaction design, Inc., San Diego, CA. (2011).
- [17] M. Baigmohammadi, V. Patel, S. Nagaraja, A. Ramalingam, S. Martinez, S. Panigrahy, A.A.E.S. Mohamed, K.P. Somers, U. Burke, K.A. Heufer, A. Pekalski, H.J. Curran, Comprehensive experimental and simulation study of the ignition delay time characteristics of binary blended methane, ethane, and ethylene over a wide range of temperature, pressure, equivalence ratio, and dilution, *Energy Fuels* 34 (2020) 3755–3771, doi:10.1021/acs.energyfuels.0c00960.
- [18] N. Lokachari, S. Panigrahy, G. Kukkadapu, G. Kim, S.S. Vasu, W.J. Pitz, H.J. Curran, The influence of isobutene kinetics on the reactivity of di-isobutylene and ISO-octane, *Combust. Flame*. 222 (2020) 186–195, doi:10.1016/j.combustflame.2020.08.007.
- [19] Y. Wu, S. Panigrahy, A.B. Sahu, C. Bariki, J. Beeckmann, J. Liang, A.A.E. Mohamed, S. Dong, C. Tang, H. Pitsch, Z. Huang, H.J. Curran, Understanding the antagonistic effect of methanol as a component in surrogate fuel models: a case study of methanol/*n*-heptane mixtures, *Combust. Flame* 226 (2021) 229–242.
- [20] G. Van Rossum, Python programming language, *USENIX Annu. Tech. Conf.* 41 (2007) 36.
- [21] D.G. Goodwin, H.K. Moffat, R.L. Speth, Cantera: an object-oriented software toolkit for chemical kinetics, thermodynamics, and transport processes, Caltech, Pasadena, CA. (2009).
- [22] S.C. Moldoveanu, Pyrolysis of organic molecules: applications to health and environmental issues, 2018. 10.1016/C2016-0-05137-9.